Applied Catalysis B: Environmental 183 (2016) 254–262

Contents lists available at ScienceDirect

Applied Catalysis B: Environmental

journal homepage: www.elsevier.com/locate/apcatb

Advanced photocatalytic performance of graphene-like BN modified BiOBr flower-like materials for the removal of pollutants and mechanism insight

Jun Di [a], Jiexiang Xia [a,*], Mengxia Ji [a], Bin Wang [a], Sheng Yin [a], Qi Zhang [a,c], Zhigang Chen [b], Huaming Li [a,*]

[a] School of Chemistry and Chemical Engineering, Institute for Energy Research, Jiangsu University, 301 Xuefu Road, Zhenjiang 212013, PR China
[b] School of the Environment, Jiangsu University, Zhenjiang 212013, PR China
[c] Hainan Provincial Key Lab of Fine Chemistry, Hainan University, Haikou 570228, PR China

ARTICLE INFO

Article history:
Received 19 August 2015
Received in revised form 14 October 2015
Accepted 18 October 2015
Available online 21 October 2015

Keywords:
Graphene-like BN
BiOBr
Photocatalytic
Visible light

ABSTRACT

Novel graphene-like BN modified BiOBr materials have been synthesized via an ionic liquid assisted solvothermal process. The structure, morphology, optical and electronic properties were explored by the XRD, XPS, FT-IR, SEM, TEM, DRS, PL, EIS and photocurrent. The photocatalytic performance of the graphene-like BN/BiOBr materials was evaluated by the degradation of colorless antibiotic agent ciprofloxacin (CIP), tetracycline hydrochloride (TC) and rhodamine B (RhB) under visible light irradiation. When the mass fraction of graphene-like BN is 1%, the graphene-like BN/BiOBr materials exhibited the highest activity. The enhanced light harvesting ability and higher separation efficiency of photogenerated electron–hole pairs by the modification of graphene-like BN contributed to the higher photocatalytic activity. The photo-degradation is dominant by the $O_2^{\bullet-}$ and hole oxidation process. This exploration of graphene-like BN modified BiOBr open a window for the use of other graphene-like BN based composites in photocatalysis field.

1. Introduction

Recently, as a conceptually-new class of materials (graphene-like materials), the two-dimensional (2D) nanomaterials with atomically ultrathin thickness have attracted increasingly research interest [1]. Since the highly anisotropic of the graphene-like structure materials exhibited the quantum confinement effect and surface effect, it can not only exhibiting enhanced intrinsic properties of the bulk materials but also generate new properties that the corresponding bulk materials do not have. Due to the broad application prospects in the biological, energy storage and conversion fields, it has aroused wide range of interests of scientists to study [2–5].

In the photocatalysis field, some graphene-like structure materials have been employed for environmental decontamination [6,7], hydrogen production from water splitting [8,9], and CO_2 reduction into hydrocarbon fuels [10]. For example, the fewer layered MoS_2 have been used as co-catalysts to improve the degradation efficiency of pollutant and hydrogen-evolution efficiency [11,12]. Wang et al. modified monolayer C_3N_4 on the surface of ZnO to improve the photocurrent and photocatalytic activity [13]. Sun et al. prepared the SnS_2 single-layers which displayed higher visible light water splitting activity compared with the bulk counterpart [14]. As the isostructural to graphite, h-BN is in the spotlight for applications as a filler for composites, a substrate for graphene electronics, in graphene-BN hybrid devices, and a support for catalysis [15]. When the thickness of BN decreased to atomically, the graphene-like BN may exhibit many special properties, such as half metallicity, modulative electrical and magnetic properties etc [16,17]. However, there have rarely report for the graphene-like structure BN used in photocatalysis field. It is highly desirable to construct graphene-like BN based composite in order to acquire efficient photocatalytic performance.

As a novel layered semiconductor material, bismuth oxybromide (BiOBr) have attracted much attention due to its unique and excellent electrical property, suitable energy band positions and excellent visible light photocatalytic performance [18–20]. It is characterized by $[Bi_2O_2]$ slabs interleaved with double slabs of bromine atoms, which result in the self-built internal static electric fields along [001] orientation and thus efficient photocatalytic activity [21]. However, the photocatalytic activity of pure BiOBr is limited by its low efficiency of light absorption,

* Corresponding authors. Fax: +86 511 88791108.
E-mail addresses: xjx@ujs.edu.cn (J. Xia), lhm@ujs.edu.cn (H. Li).

http://dx.doi.org/10.1016/j.apcatb.2015.10.036
0926-3373/

low adsorption capacity and high recombination rate of photo-induced electron–hole pairs [22]. Therefore, several strategies have been employed to improve the photocatalytic performance of BiOBr materials. Firstly, preparing materials with specific structures, such as ultrathin nanosheets [23], flower-like structure [24] and hollow microspheres [25]. Secondly, performing dehalogenation to regulate the chemical compositions such as Bi_3O_4Br [26], $Bi_4O_5Br_2$ [27] and $Bi_{24}O_{31}Br_{10}$ [28]. Thirdly, surface functionalization or producing oxygen vacancies [29,30]. Fourthly, coupling with different semiconductor to build hybrid materials, such as Ag/AgBr/BiOBr [31], BiOBr@SiO_2@Fe_3O_4 [32], Cu_2O/BiOBr [33], BiOBr-BiOI [34], BiOBr-TiO_2-graphene [35], BiOBr-g-C_3N_4 [36], and BiOBr/$Bi_{24}O_{31}Br_{10}$ [37]. Considering the superiority of graphene-like BN and BiOBr, it may further improve the photocatalytic activity if appropriate method is adopted to couple the graphene-like BN and BiOBr with tight integration.

In this study, graphene-like BN/BiOBr materials have been prepared via an ionic liquid 1-hexadecyl-3-methylimidazolium bromide ([C_{16}mim]Br) assisted solvothermal method. The [C_{16}mim]Br could acted as Br source, template and dispersing agent at the same time. The photocatalytic activity of the as-prepared materials was evaluated by the degradation of colorless antibiotic agent ciprofloxacin (CIP), tetracycline hydrochloride (TC) and rhodamine B (RhB) under the irradiation of visible light. The key role of graphene-like BN for the improved photocatalytic performance was explored and the main active species were determined.

2. Experimental

2.1. Synthesis of the photocatalysts

The ionic liquid [C_{16}mim]Br (1-hexadecyl-3-methylimidazolium bromide) (99%) was purchased from Shanghai Chengjie Chemical Co. Ltd. All other reagents used in this research were analytically pure and used without further purification. The graphene-like BN was prepared by calcinations with boric acid and urea as reactants. The boric acid and urea with the mole ratio of 1:24 were dissolved in 40 mL distilled water and heated at 80 °C to obtained white solid. Then the obtained solid was calcined at 900 °C for 5 h under an nitrogen atmosphere [38].

A typical synthesis of graphene-like BN/BiOBr materials was as follows: 1 mmol [C_{16}mim]Br was dissolved into 20 mL ethanol which contains a certain amount of graphene-like BN. The stoichiometric amounts $Bi(NO_3)_3{\cdot}5H_2O$ was added into the above solution under stirring and further stirred for 30 min. The suspension was added in 25 mL Teflon-lined autoclave and maintained at 140 °C for 24 h. The products were washed three times with distilled water and ethanol and dried at 50 °C for 24 h.

2.2. Characterization

The crystallinity of the as-prepared sample was characterized by X-ray diffraction (XRD) on Shimadzu XRD-6000 X-ray diffractometer at room temperature. Morphologies of the prepared samples were examined with scanning electron microscopy (SEM) measurements (JEOL JSM-7001F) and transmission electron microscopy (TEM) by a JEOL JEM-2100 electron microscope operated at an accelerating voltage of 200 kV. Fourier transform infrared (FTIR) spectra were carried on a Nexus 470 spectrometer using KBr disks. X-ray photoelectron spectroscopy (XPS) data were obtained on VG MultiLab 2000 system with a monochromatized Mg-Kα line source. UV–vis diffuse reflectance spectra (DRS) of the samples were measured by using Shimadzu UV-2450 UV–vis spectrophotometer. Electrochemical impedance spectroscopy (EIS) and photocurrent measurements were performed on an electrochemical system (CHI-660B, China). It was conducted in three-electrode quartz cells with platinum wire as the counter electrode and saturated Ag/AgCl electrode as the reference electrodes, respectively. The as-prepared photocatalyst film electrodes on ITO were worked as the working electrode. The photocurrents and EIS were measured with a phosphate buffered saline (0.1 mol L^{-1}, pH 7.0) and 0.1 M KCl solutions containing 5 mM $Fe(CN)_6^{3-}$/$Fe(CN)_6^{4-}$ as electrolyte solutions, respectively. A 500 W Xe arc lamp was served as the photosource.

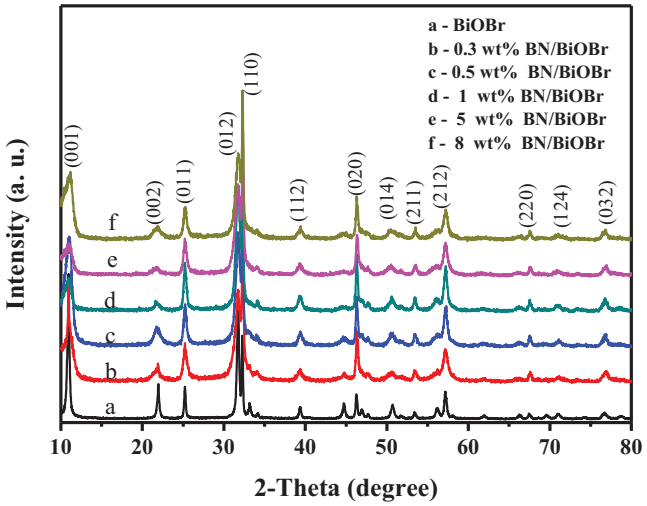

Fig. 1. XRD patterns of the obtained pure BiOBr and graphene-like BN/BiOBr composites.

2.3. Photocatalytic experiments

The photocatalytic activities were evaluated by the decomposition of rhodamine B (RhB), ciprofloxacin (CIP) and tetracycline hydrochloride (TC) under visible light irradiation (λ > 400 nm). Visible irradiation was acquired by a 300 W Xe lamp with a 400 nm cutoff filter. For the photocatalytic experiments, 10 mg, 50 mg, 50 mg of photocatalyst was totally dispersed in an aqueous solution of RhB (100 mL, 10 mg L^{-1}), CIP (100 mL, 10 mg L^{-1}) and TC (100 mL, 20 mg L^{-1}), respectively. Before irradiation, the suspensions were magnetically stirred in the dark for 30 min to reach absorption–desorption equilibrium between the photocatalyst and model pollutants. At certain time intervals, 3 mL suspension were periodically sampled and centrifuged to remove the photocatalyst particles. The concentration of RhB, CIP and TC was analyzed by a UV–vis spectrophotometer (Shimadzu, UV-2450) according to its absorbance at 553 nm, 276 nm, 356 nm, respectively.

3. Results and discussion

3.1. XRD analysis

The crystalline phases of the BiOBr and BN/BiOBr composites with different contents of BN were investigated by X-ray diffraction (XRD) (Fig. 1). BN/BiOBr composites showed the similar diffraction peaks with the pristine BiOBr. The peaks at $2\theta = 10.9^\circ$, 21.9°, 25.3°, 31.8°, 32.3°, 39.4°, 46.3°, 50.8°, 53.5°, 57.3°, 67.6°, 71.2°, 76.7° were respectively indexed to (0 0 1), (0 0 2), (0 1 1), (0 1 2), (1 1 0), (1 1 2), (0 2 0), (0 1 4), (2 1 1), (2 1 2), (2 2 0), (1 2 4), (0 3 2) crystal planes of tetragonal BiOBr (JCPDS card no. 73-2061). It was noted that no diffraction peaks of BN were found in XRD patterns. That could be the low amount BN in the BN/BiOBr composites or high dispersion of BN and the similar results can also be found in other systems [39,40].

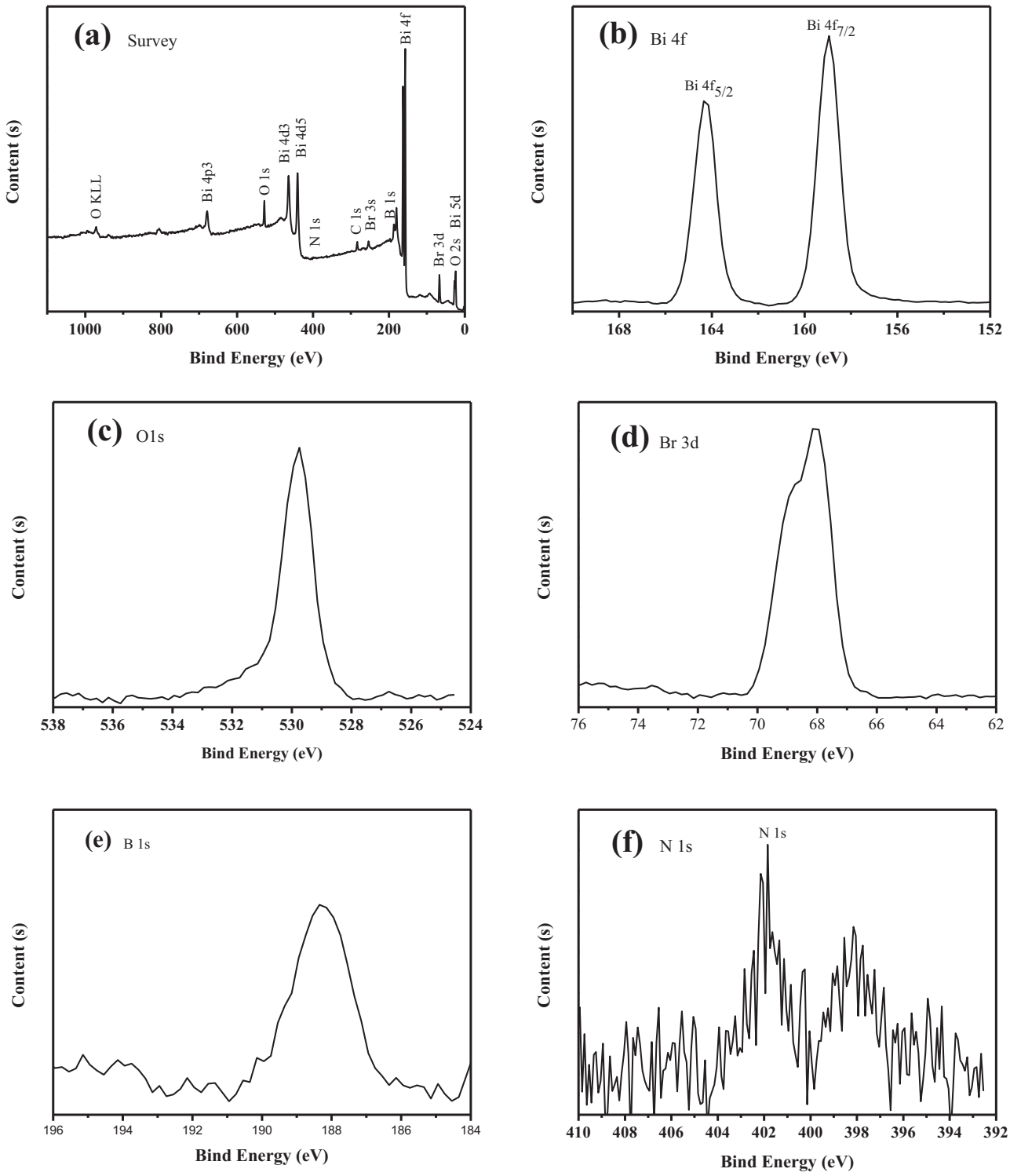

Fig. 2. XPS spectra of the 1 wt% graphene-like BN/BiOBr composite. (a) Survey of the sample; (b) Bi 4f; (c) O 1s; (d) Br 3d; (e) B 1s and (f) N 1s.

3.2. XPS analysis

XPS, being very sensitive response to the chemical state of materials surface, is usually used to confirm the element and valence. In the survey scan spectrum of BN/BiOBr composite (Fig. 2a), Bi, O, Br, B, and N are all observed, which is chemical composition of the composite material. As for the high resolution of Bi 4f (Fig. 2b), two peaks at 159.1 and 164.5 eV can be seen, which is ascribed to the Bi $4f_{7/2}$ and Bi $4f_{5/2}$ respectively, and is the characteristic of Bi^{3+}. The peaks at 529.9 and 68.3 eV are assigned to O 1s and Br 3d, respectively (Fig. 2c and d). With regard to B 1s and N 1s (Fig. 2e and f), this demonstrates that BN has been successfully attached on BiOBr.

3.3. FT-IR analysis

The existence of BN in the BN/BiOBr materials is further certified by FT-IR analysis. Fig. 3 shows the FT-IR spectra of the BiOBr and BN/BiOBr samples with different contents. The aborption peaks

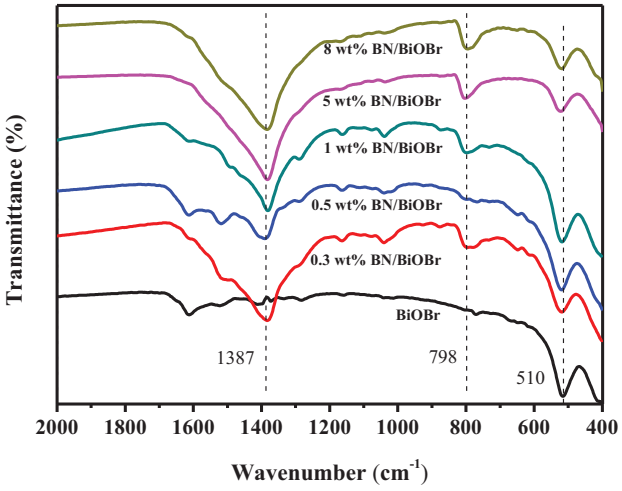

Fig. 3. FT-IR of graphene-like BN/BiOBr composites with different contents of BN.

at 1387 and 798 cm^{-1} could be observed, which ascribed to the in-plane B—N stretching vibration and the B—N—B out-of-plane bending vibration, respectively [41,42]. BiOBr exhibited the Bi—O stretching mode at 510 cm^{-1}. For comparison, the Bi—O bands could also be found in BN/BiOBr composites but the positions showed slightly shift, which indicate there has an interaction between BN and BiOBr. Therefore, the FT-IR results provided further evidences that BN was successfully coupled with BiOBr and the interaction existed between BN and BiOBr.

3.4. SEM and TEM analysis

The morphology and superficial microstructure of BN/BiOBr materials was characterized by scanning electron microscopy (SEM) and transmission electron microscopy (TEM). Fig. 4 shows the SEM and TEM images of pure BN, and BN/BiOBr composites. In Fig. 4a, the pure BN exhibited a near transparency of the sheets and a silk-like nanostructure, indicating the graphene-like ultra-thin thickness. In EDS pattern, B, N, O, Br, and Bi elements could be observed (Fig. 4b), which proved that the as-prepared sample was BN/BiOBr composite. The graphene-like BN weight content in

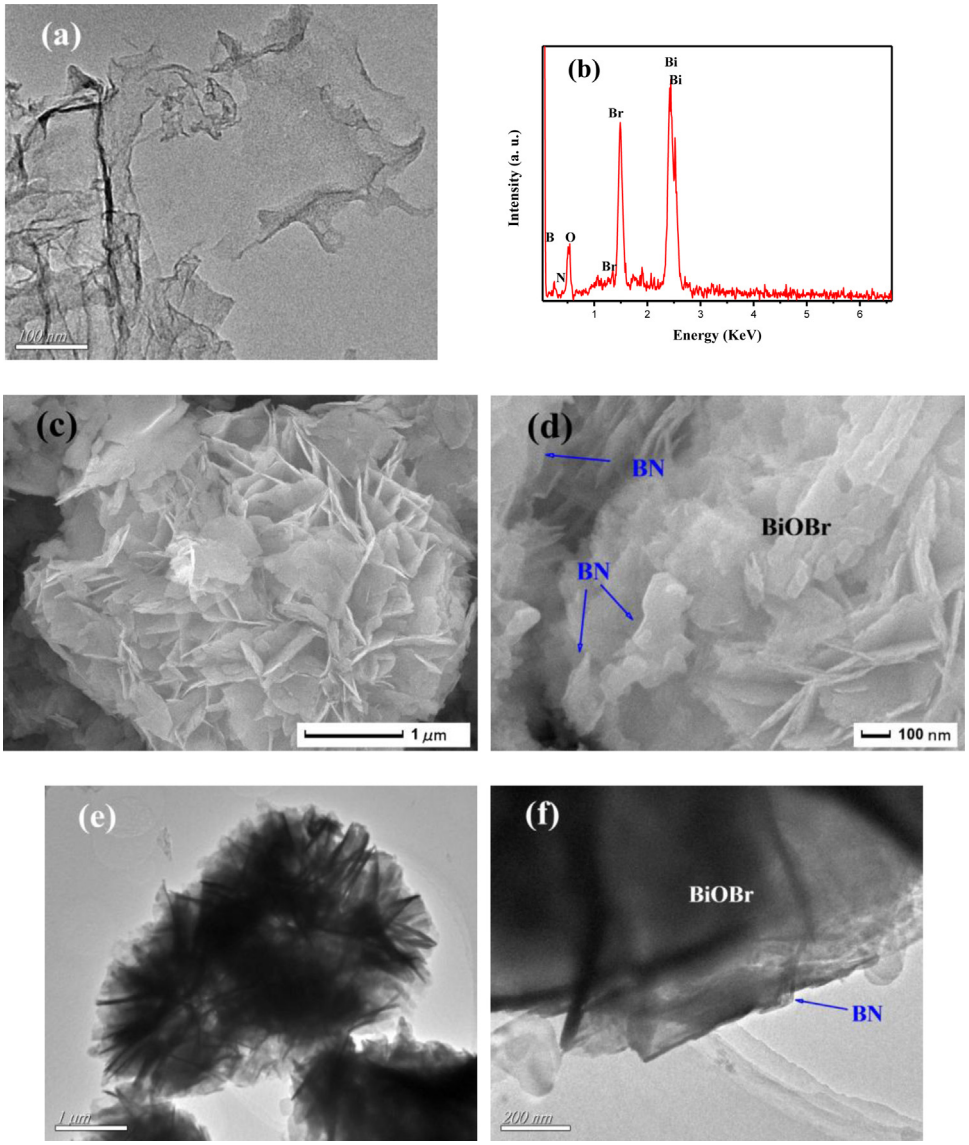

Fig. 4. (a) TEM image of graphene-like BN; (b) EDS of the 1 wt% graphene-like BN/BiOBr; (c and d) SEM images of 1 wt% graphene-like BN/BiOBr; (e amd f) TEM images of 1 wt% graphene-like BN/BiOBr.

BN/BiOBr composite materials was determined by EDS analysis. There has 0.8 wt% graphene-like BN in the 1 wt% BN/BiOBr materials and 6.4 wt% graphene-like BN in the 8 wt% BN/BiOBr materials, respectively. The weight contents of graphene-like BN determined by EDS analysis was close to the contents initial added. Fig. 4c and d are the SEM images of BN/BiOBr composite. As shown in the SEM images, BN/BiOBr composite had flower-like structure with self-assembly by nanosheet. And the BN on the surface of BiOBr materials can be seen, which revealing the BN and BiOBr have been coupled successfully. The TEM image further revealed the flower-like microspheres structure of BN/BiOBr composite (Fig. 4e) and is consistent with the SEM analysis. The BN on the surface of BiOBr can also be found with tight contacted with each other (Fig. 4f). EDS element mapping clearly showed the elements B, N, O, Bi and Br evenly distributed in graphene-like BN/BiOBr (Fig. S1).

3.5. Optical absorption properties

The optical absorption spectra were used to explore the effect of BN modification on the electronic structure of BiOBr. The obtained materials exhibited the typical absorption patterns of semiconductors and the result is shown in Fig. 5. The optical absorption of graphene-like BN/BiOBr materials in the visible light region was enhanced and the absorption edge exhibited somewhat red-shift when compared to pure BiOBr. The band gap of BN/BiOBr composites was estimated via the classical Tauc approach. As shown in Fig. 5b, the band gap of BN/BiOBr materials became smaller after the BN was introduced to the BiOBr. This graphene-like BN modification to the BiOBr narrows the material band gap and improves the ability of the material to harvest visible light which favors the higher photocatalytic performance [43].

3.6. Nitrogen adsorption analysis

To characterize the specific surface area of the obtained catalysts, the nitrogen adsorption and desorption isotherms were carried out (Fig. S2). The BET specific surface area of BiOBr, 0.3 wt% BN/BiOBr, 0.5 wt% BN/BiOBr, 1 wt% BN/BiOBr, 5 wt% BN/BiOBr and 8 wt% BN/BiOBr was calculated to be 17.15 $m^2 g^{-1}$, 18.03 $m^2 g^{-1}$, 18.16 $m^2 g^{-1}$, 19.10 $m^2 g^{-1}$, 19.61 $m^2 g^{-1}$ and 20.57 $m^2 g^{-1}$, respectively. The BET surface areas of the graphene-like BN/BiOBr composites are similarly. It is known that the larger specific surface areas can absorb more active species and reactants on its surface. In this system, the BET surface area may be not the main factors to determining the photocatalytic activity.

3.7. Photocatalytic performance

To assess the photocatalytic activity of BN/BiOBr composite, the variation of the degree of degradation (C/C_0) with time was plotted for 10 mg/L RhB (Fig. 6a). As shown in Fig. S2, the absorption–desorption balance have been achieved between the catalyst and pollutant for 30 min absorption process. In comparison to pure BiOBr, the degrees of degradation for BN/BiOBr composites were all significantly enhanced. Notably, the 1 wt% BN/BiOBr composite exhibited the best photocatalytic activity. After irradiation for 30 min under visible light, the degree of RhB degradation could reach 99%. For comparison, the photocatalytic activity of graphene modified BiOBr materials which prepared via the same method was also investigated. The 1 wt% graphene-like BN/BiOBr materials also displayed higher photocatalytic activity than 1 wt% graphene/BiOBr sample. When the content of graphene-like BN was higher than 1 wt%, a further increase of graphene-like BN content caused a decrease in the photocatalytic activity of RhB degradation. This was attributed to that although the modification of graphene-like BN favored the charge separation, while too many graphene-like BN

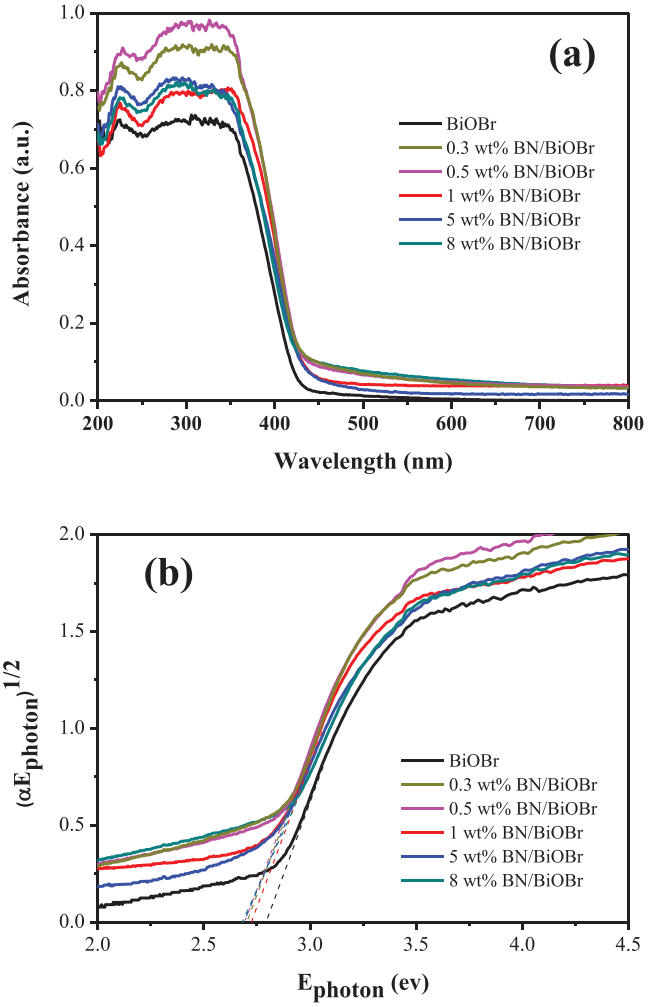

Fig. 5. (a) The UV–vis absorption spectra and (b) $(\alpha E_{photon})^{1/2}$ vs. E_{photon} curves for the obtained pure BiOBr and graphene-like BN/BiOBr composites.

covered on the surface of BiOBr would shielding the BiOBr from absorbing visible light. The lower light harvesting could reduce the generation of electron–hole pairs. Therefore, too much content of graphene-like BN could lead to the decrease of photocatalytic activity. Fig. 6b shows the variation of UV–vis absorption spectrum of RhB degradation. The intensity of the absorption peak decreased as the time increased. Simultaneously, it obviously observed that the maximum absorption peak of RhB was blue-shifted, which was attributed to the step-by-step de-ethylation process [44]. A total organic carbon (TOC) experiment has been carried out for the degradation of RhB by 1 wt% graphene-like BN/BiOBr under visible light irradiation (Fig. S3). After irradiation for 120 min, 66.2% of RhB was mineralized, which indicating the RhB can be degraded by graphene-like BN/BiOBr under visible light irradiation. To test the stability of the graphene-like BN/BiOBr materials, the 1 wt% BN/BiOBr material was collected after photodegradation experiment of RhB. As shown in Fig. S4, the photocatalytic activity could still be maintained after four cycles with only 5.6% decrease of the degradation efficiency. To further confirm the stability of the graphene-like BN/BiOBr material, we compare the XRD of the 1 wt% BN/BiOBr sample before and after experiments (Fig. S5). The results reveal that the crystal structures of the graphene-like BN/BiOBr do not change after the photocatalytic reaction.

Antibiotic agent has been widely used in a variety of human and veterinary applications, which may pose serious threats to the ecosystem and human health by inducing proliferation of bacterial

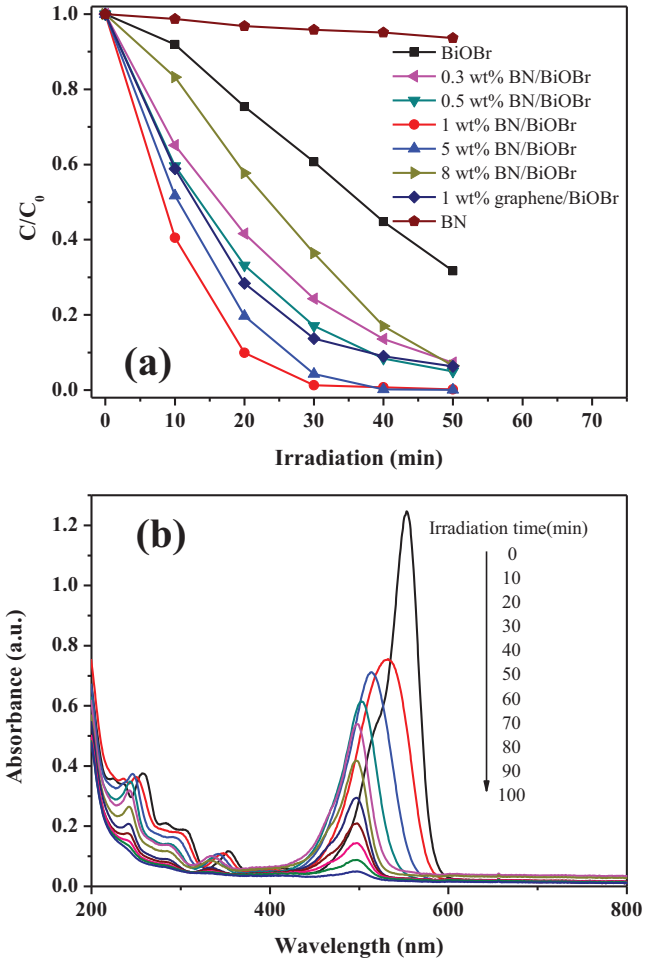

Fig. 6. (a) Photodegradation of RhB by BiOBr and graphene-like BN/BiOBr composites under visible light irradiation; (b) time-dependent UV–vis absorption spectra in the presence of 1 wt% graphene-like BN/BiOBr.

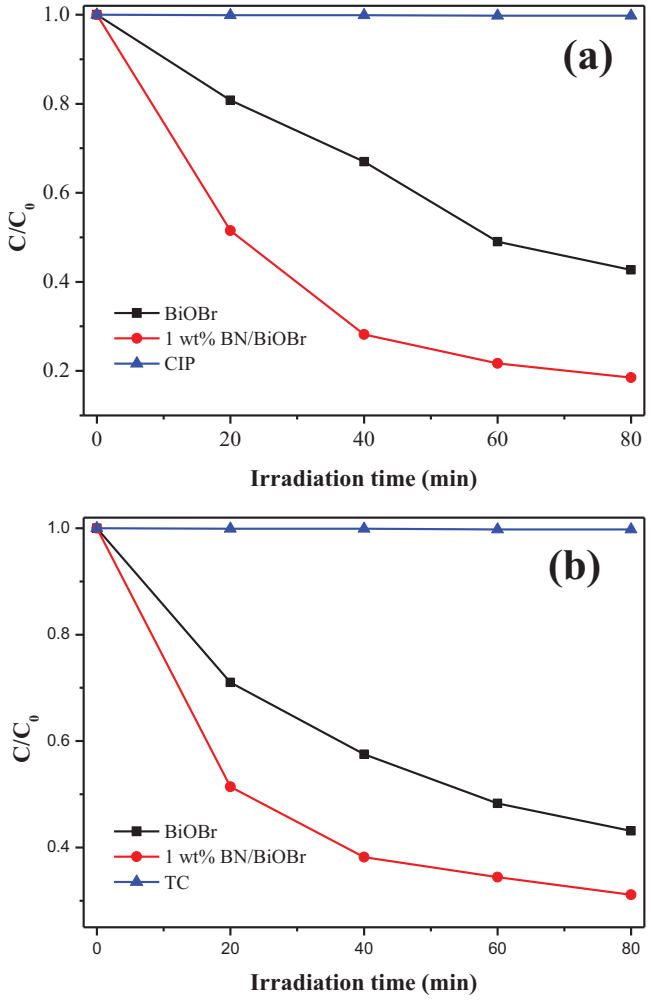

Fig. 7. Photocatalytic degradation of (a) CIP and (b) TC in the presence of pure BiOBr, 1 wt% graphene-like BN/BiOBr under visible light irradiation.

drug resistance even in small concentrations or with low residual activity. Therefore, the removal of antibiotic agent from aqueous solution is of great significant. Ciprofloxacin (CIP) and tetracycline (TC) were selected as typical antibiotic agents for evaluating the photocatalytic activity of BN/BiOBr materials under visible light irradiation. As shown in Fig. 7, the blank test indicated that the self-photolysis of CIP and TC can be ignored. It is seen that BN/BiOBr composite exhibited higher photocatalytic activity for CIP and TC degradation as compared to pure BiOBr. After visible light irradiation for 80 min, 81.5% of CIP was degraded by 1 wt% BN/BiOBr and only 57.3% of CIP can be degraded by pure BiOBr (Fig. 7a). As for the TC degradation, the enhanced photocatalytic activity can also be found after BN was modified on the BiOBr materials (Fig. 7b). The results of photocatalytic degradation indicate the BN/BiOBr composite was effective photocatalyst for antibiotic agent removal.

3.8. Electrochemistry analysis

The photocurrent responses of pure BiOBr and 1% BN/BiOBr composite are presented in Fig. 8. The photocurrent intensity stays a stable value when the light is on, and rapidly returns to dark current state if the light is turned off. The photocurrent is formed by separation and transportation of the photoinduced charges to the working electrodes. In view of photocurrent density of pure BiOBr and 1% BN/BiOBr composite, 1% BN/BiOBr composite showed higher current than pure BiOBr, indicating higher separation efficiency of electrons and holes and longer lifetime of charge carriers photogenerated over 1% BN/BiOBr composite than pure BiOBr [45].

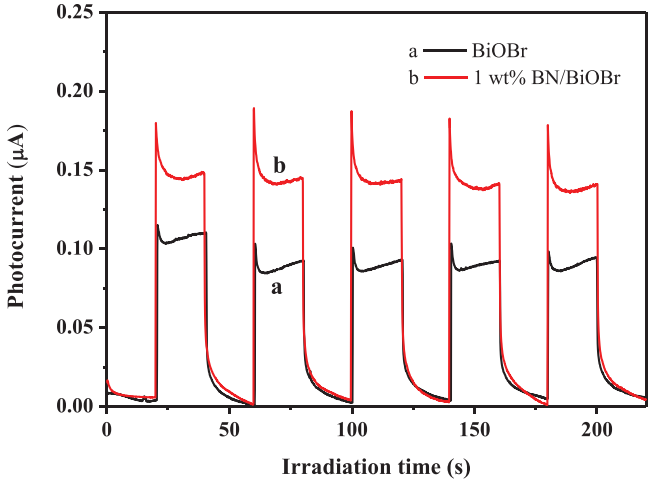

Fig. 8. Transient photocurrent response of the sample electrodes of pure BiOBr and 1 wt% graphene-like BN/BiOBr composites.

The zeta-potential of the commercial BN and the graphene-like BN materials was tested. The zeta-potential of commercial BN dispersions in water was −28 mV, while that of graphene-like BN was

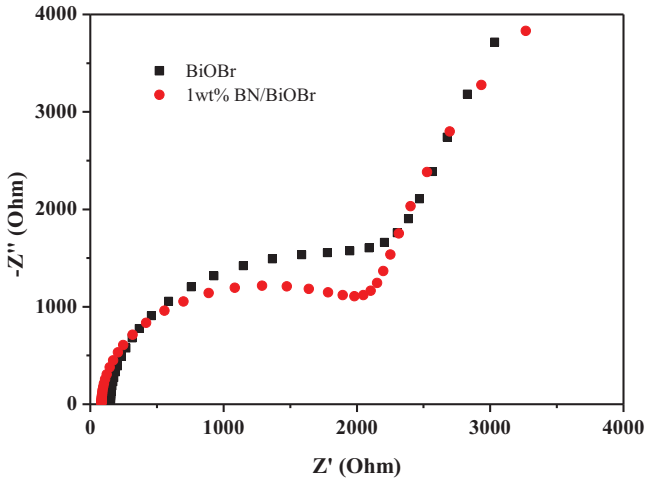

Fig. 9. Electrochemical impedance spectroscopy (EIS) Nyquist plots of the sample electrodes of pure BiOBr and 1 wt% graphene-like BN/BiOBr composites.

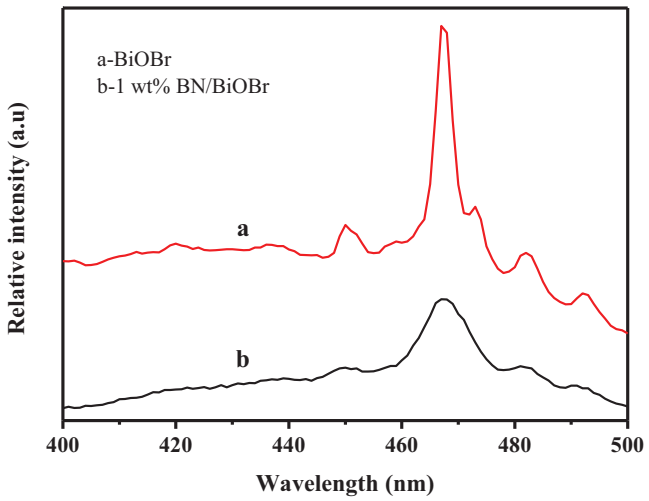

Fig. 10. Photoluminescence spectra of the obtained pure BiOBr and 1 wt% graphene-like BN/BiOBr composites.

−35 mV. The graphene-like BN showed a more negative potential which indicated that it could absorb more electrons on its surface when the thickness of BN decreased to the atomically ultrathin structure [46]. The h-BN is a layered structure comprising alternating boron and nitrogen atoms in a honeycomb arrangement. Boron atoms are sp^2 hybridized with electron-deficient virtual orbitals [47]. The nitrogen atoms in the internal layers provide electrons to the boron atoms in the adjacent layers, which indicates that the BN sample with an atomically thickness could improve the electronic absorption ability for the virtual orbitals in boron atoms [48]. Therefore, the graphene-like BN materials in this system display higher electron absorbing ability. Due to the graphene-like BN and BiOBr have analogous layered structures, the lattice mismatch can be minimized, and heterojunctions with intimate contacts can be constructed. It can increase the accessible area of the graphene-like BN and BiOBr planar interface and reduce the barrier to electron transfer, thus accelerating the interfacial charge transfer process by the electron tunneling effect [49]. Thus, the better separation efficiency of electron–hole pairs in the graphene-like BN/BiOBr can be obtained.

To further demonstrate the superiority of 1% BN/BiOBr composite over pure BiOBr in the charge carrier transfer, EIS measurements were investigated. 1% BN/BiOBr composite shows the smaller diameter of the Nyquist circle than that of pure BiOBr as shown in Fig. 9, suggesting that 1% BN/BiOBr composite has a lower charge transfer resistance and more effective electron–hole pair separation [50].

3.9. PL spectra

Fig. 10 shows the photoluminescence (PL) spectra of BiOBr and BN/BiOBr composite. Since PL is related to recombination of electron–hole and emission of photons. A weaker intensity of the PL implies lower efficiency of electrons and holes recombination. As the Fig. 10 shown, due to the introduction of BN, the intensity of PL for BN/BiOBr composite decreased when compared to the pure BiOBr. The result demonstrated that the higher separation efficiency of electron–hole pairs is achieved over the BN/BiOBr composite.

3.10. ESR analysis

In order to investigate the effect for the active species by graphene-like BN modification, the electron spin resonance (ESR) spin-trap technique was carried out. As shown in Fig. 11a, four characteristic peaks of DMPO-$O_2^{\bullet-}$ were observed in the methanol dispersion of pure BiOBr under visible light irradiation, which implying the $O_2^{\bullet-}$ radical species were produced via single-electron reduction process. No DMPO-$^{\bullet}$OH signal were observed, indicating the $^{\bullet}$OH may be not the main active species during the photocatalysis process (Fig. 11b). Furthermore, after the graphene-like BN was modified on the BiOBr materials, no distinct difference was observed for both the $O_2^{\bullet-}$ and $^{\bullet}$OH radical species (Fig. 11c and d). This result revealed the modification of graphene-like BN may not affect the type or the amount of main active species, and the active species variation may not the mainly reason for the improvement of photocatalytic activity.

3.11. Radical trapping experiments

Radicals trapping experiments are further conducted to determine the reactive active species generated during the irradiation of the 1% BN/BiOBr material. During the experiments, EDTA was used as holes radical scavenger and *tert*-butanol as hydroxyl radical scavenger [51]. As shown in Fig. 12, the addition of EDTA restrains the photocatalytic activity of 1% BN/BiOBr material significantly. Simultaneously, it can be observed that *tert*-butanol had a little influence for photocatalytic activity and it was in accordance with the ESR analysis. The above results indicated $O_2^{\bullet-}$ and holes were the main active species for the photodegradation process.

Based on the analysis above mentioned, the significant enhancement of photocatalytic activity for the degradation of pollutants could be attributed to the synergistic effect between graphene-like BN and BiOBr material. As shown in Fig. 13, the electrons can be excited from the VB to the CB to form photo-generated electron–hole pairs when the BiOBr is irradiated by visible light. Based on the DRS analysis, the introduction of graphene-like BN to the BiOBr improves the visible light harvesting ability and narrowed the band gap which beneficial for the formation of more electron–hole pairs. When no graphene-like BN was modified on the BiOBr, the generated charge carriers cannot be effective spatial separated and large portion of charge carriers would recombine. However, when the graphene-like BN was modified, the photo-generated electrons can be effective collected by graphene-like BN and further reduce the adsorbed O_2 to $O_2^{\bullet-}$. For the RhB degradation, the RhB dye could absorb the visible light to produce singlet and triplet states (denoted as RhB*) and the excited electron could inject into the CB of BiOBr [52]. The electron on the CB of BiOBr could migrate to the graphene-like BN and result in effective separation. The formed holes and $O_2^{\bullet-}$ acted as the active species and play cru-

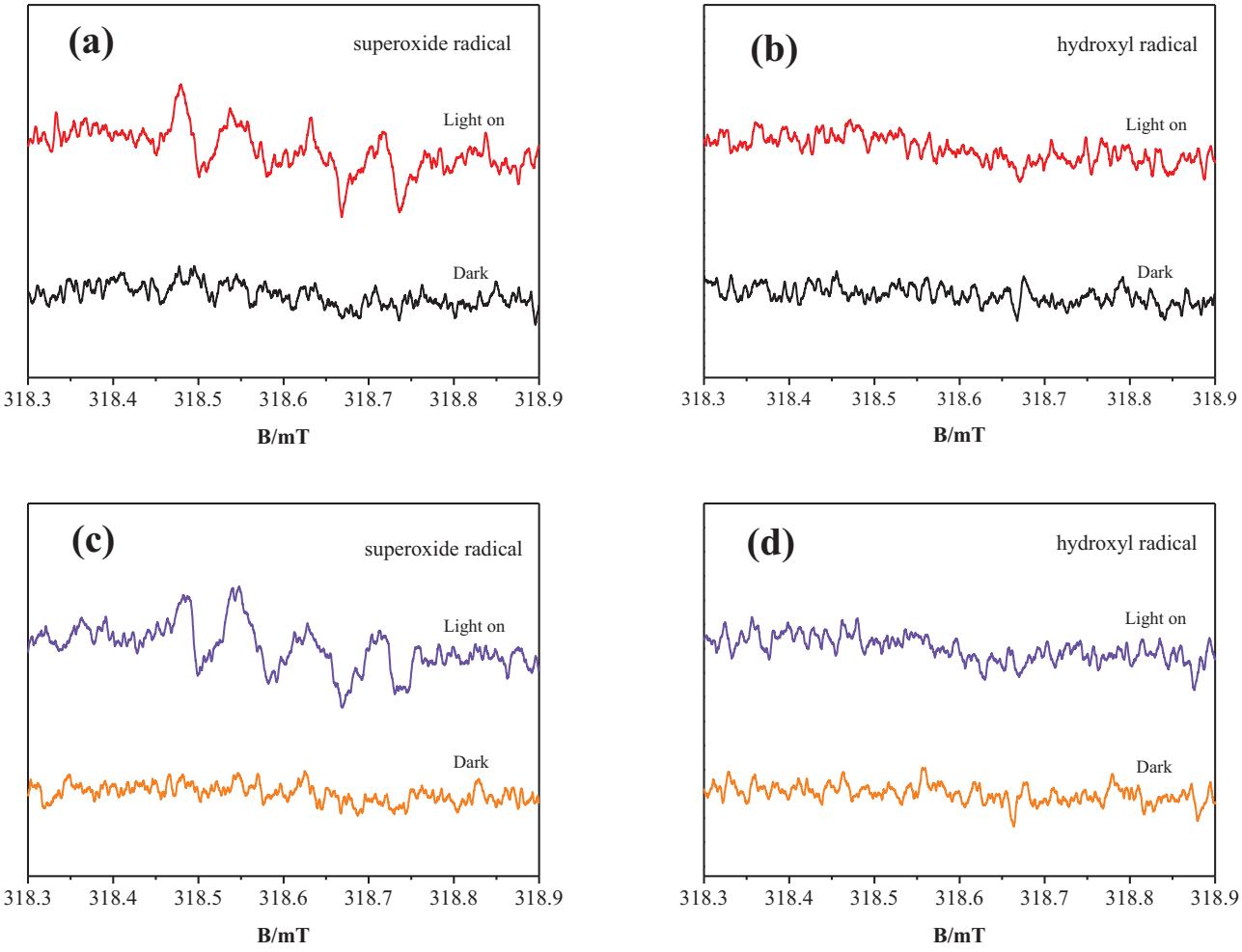

Fig. 11. DMPO spin-trapping ESR spectra recorded with (a and b) pure BiOBr and (c and d) 1 wt% graphene-like BN/BiOBr samples in (a and c) methanol dispersion (for DMPO-$O^{\bullet -}$) and (b and d) aqueous dispersion (for DMPO-$^{\bullet}OH$) under visible light irradiation.

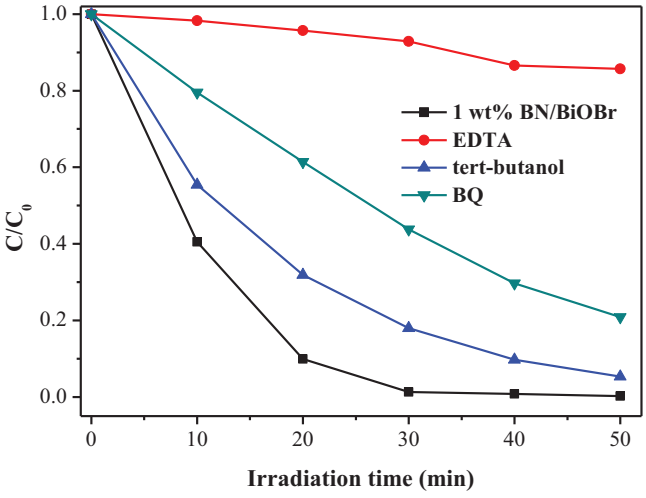

Fig. 12. Comparison of the photocatalytic activities of 1 wt% graphene-like BN/BiOBr composites for the degradation of RhB with or without adding EDTA-2Na, *tert*-butanol and BQ under visible light irradiation.

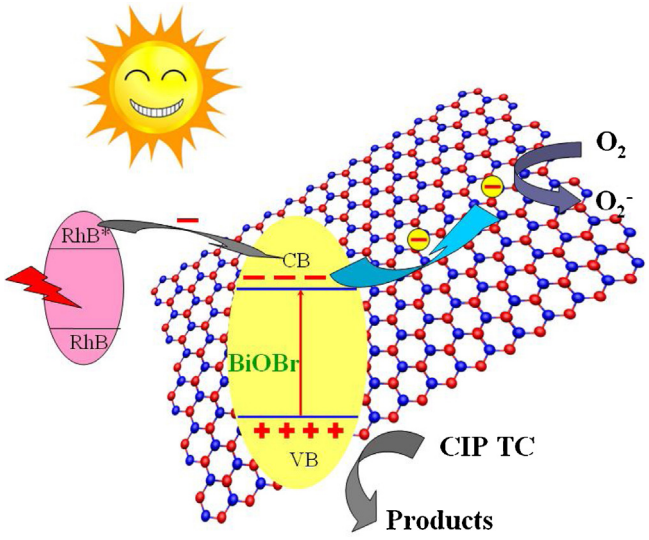

Fig. 13. Schematic of the separation and transfer of photogenerated charges in the graphene-like BN/BiOBr materials combined with the possible reaction mechanism of the photocatalytic procedure.

cial role during the photodegradation process. The graphene-like BN modification endow higher separation efficiency of photogenerated electron–hole pairs for BN/BiOBr materials which leading to better photocatalytic activity.

4. Conclusions

In summary, graphene-like BN/BiOBr materials have been prepared via a facile solvothermal process in the presence of the

ionic liquid [C_{16}mim]Br. The graphene-like BN was well-dispersed on the BiOBr materials and tight contact interface has been constructed. The graphene-like BN/BiOBr materials displayed higher photocatalytic activity for the degradation of RhB, CIP and TC. The effect of different addition contents of graphene-like BN on the photocatalytic activity of graphene-like BN/BiOBr materials was systematically investigated. The enhanced photocatalytic activity was attributed to the improved visible light harvesting ability and higher separation efficiency of photogenerated electron–hole pairs by the introduction of graphene-like BN. The graphene-like BN/BiOBr materials with high photocatalytic activity could be beneficial to industrial applications to eliminate the organic pollutants from waste water.

Acknowledgements

This work was financially supported by the National Nature Science Foundation of China (Nos. 21206060, 21476098 and 21471069), Jiangsu Province (1102118C), and the Special Financial Grant from the China Postdoctoral Science Foundation (2013T60506).

Appendix A. Supplementary data

Supplementary data associated with this article can be found, in the online version, at http://dx.doi.org/10.1016/j.apcatb.2015.10.036.

References

[1] Y.F. Sun, S. Gao, Y. Xie, Chem. Soc. Rev. 43 (2014) 530–546.
[2] C.L. Tan, H. Zhang, Chem. Soc. Rev. 44 (2015) 2713–2731.
[3] M.S. Xu, T. Liang, M.M. Shi, H.Z. Chen, Chem. Rev. 113 (2013) 3766–3798.
[4] Y.F. Sun, S. Gao, F.C. Lei, C. Xiao, Y. Xie, Acc. Chem. Res. 48 (2015) 3–12.
[5] L. Liang, K. Li, C. Xiao, S.J. Fan, J. Liu, W.S. Zhang, W.H. Xu, W. Tong, J.Y. Liao, Y.Y. Zhou, B.J. Ye, Y. Xie, J. Am. Chem. Soc. 137 (2015) 3102–3108.
[6] Q.Y. Lin, L. Li, S.J. Liang, M.H. Liu, J.H. Bi, L. Wu, Appl. Catal. B 163 (2015) 135–142.
[7] M.L. Guan, C. Xiao, J. Zhang, S.J. Fan, R. An, Q.M. Cheng, J.F. Xie, M. Zhou, B.J. Ye, Y. Xie, J. Am. Chem. Soc. 135 (2013) 10411–10417.
[8] S.B. Yang, Y.J. Gong, J.S. Zhang, L. Zhan, L.L. Ma, Z.Y. Fang, R. Vajtai, X.C. Wang, P.M. Ajayan, Adv. Mater. 25 (2013) 2452–2456.
[9] Z.Z. Lin, X.C. Wang, Angew. Chem. Int. Ed. 52 (2013) 1735–1738.
[10] S. Bai, X.J. Wang, C.Y. Hu, M.L. Xie, J. Jiang, Y.J. Xiong, Chem. Commun. 50 (2014) 6094–6097.
[11] Q.J. Xiang, J.G. Yu, M. Jaroniec, J. Am. Chem. Soc. 134 (2012) 6575–6578.
[12] J. Di, J.X. Xia, Y.P. Ge, L. Xu, H. Xu, J. Chen, M.Q. He, H.M. Li, Dalton Trans. 43 (2014) 15429–15438.
[13] Y.J. Wang, R. Shi, J. Lin, Y.F. Zhu, Energy Environ. Sci. 4 (2011) 2922–2929.
[14] Y.F. Sun, H. Cheng, S. Gao, Z.H. Sun, Q.H. Liu, Q. Liu, F.C. Lei, T. Yao, J.F. He, S.Q. Wei, Y. Xie, Angew. Chem. Int. Ed. 51 (2012) 8727–8731.
[15] X.F. Song, J.L. Hu, H.B. Zeng, J. Mater. Chem. C 1 (2013) 2952–2969.
[16] L. Ma, H. Hu, L. Zhu, J. Wang, J. Phys. Chem. C 115 (2011) 6195–6199.
[17] Y. Wang, Y. Ding, J. Ni, J. Phys. Chem. C 116 (2012) 5995–6003.
[18] J. Li, Y. Yu, L.Z. Zhang, Nanoscale 6 (2014) 8473–8488.
[19] J.X. Xia, J. Di, S. Yin, H. Xu, J. Zhang, Y.G. Xu, L. Xu, H.M. Li, M.X. Ji, RSC Adv. 4 (2014) 82–90.
[20] H.F. Cheng, B.B. Huang, Y. Dai, Nanoscale 6 (2014) 2009–2026.
[21] J. Di, J.X. Xia, Y.P. Ge, L. Xu, H. Xu, M.Q. He, Q. Zhang, H.M. Li, J. Mater. Chem. A 2 (2014) 15864–15874.
[22] J. Di, J.X. Xia, S. Yin, H. Xu, M.Q. He, H.M. Li, L. Xu, Y.P. Jiang, RSC Adv. 3 (2013) 19624–19631.
[23] J. Chen, M.L. Guan, W.Z. Cai, J.J. Guo, C. Xiao, G.K. Zhang, Phys. Chem. Chem. Phys. 16 (2014) 20909–20914.
[24] Y.N. Huo, J. Zhang, M. Miao, Y. Jin, Appl. Catal. B 111–112 (2012) 334–341.
[25] J.X. Xia, S. Yin, H.M. Li, H. Xu, L. Xu, Y.G. Xu, Dalton Trans. 40 (2011) 5249–5258.
[26] J.L. Wang, Y. Yu, L.Z. Zhang, Appl. Catal. B 136–137 (2013) 112–121.
[27] J. Di, J.X. Xia, M.X. Ji, S. Yin, H.P. Li, H. Xu, Q. Zhang, H.M. Li, J. Mater. Chem. A 3 (2015) 15108–15118.
[28] J. Shang, W.C. Hao, X.J. Lv, T.M. Wang, X.L. Wang, Y. Du, S.X. Dou, T.F. Xie, D.J. Wang, J.O. Wang, ACS Catal. 4 (2014) 954–961.
[29] J.X. Xia, J. Di, H.T. Li, H. Xu, H.M. Li, S.J. Guo, Appl. Catal. B 181 (2016) 260–269.
[30] H. Li, J. Shang, Z.H. Ai, L.Z. Zhang, J. Am. Chem. Soc. 137 (2015) 6393–6399.
[31] H.F. Cheng, B.B. Huang, P. Wang, Z.Y. Wang, Z.Z. Lou, J.P. Wang, X.Y. Qin, X.Y. Zhang, Y. Dai, Chem. Commun. 47 (2011) 7054–7056.
[32] L. Zhang, W.Z. Wang, S.M. Sun, Y.Y. Sun, E.P. Gao, Z.J. Zhang, Appl. Catal. B 148–149 (2014) 164–169.
[33] W.Q. Cui, W.J. An, L. Liu, J.S. Hu, Y.H. Liang, J. Hazard. Mater. 280 (2014) 417–427.
[34] H.W. Huang, X. Han, X.W. Li, S.C. Wang, P.K. Chu, Y.H. Zhang, ACS Appl. Mater. Interfaces 7 (2015) 482–492.
[35] X.X. Wei, C.M. Chen, S.Q. Guo, F. Guo, X.M. Li, X.X. Wang, H.T. Cui, L.F. Zhao, W. Li, J. Mater. Chem. A 2 (2014) 4667–4675.
[36] L.Q. Ye, J.Y. Liu, Z. Jiang, T.Y. Peng, L. Zan, Appl. Catal. B 142–143 (2013) 1–7.
[37] F.T. Li, Q. Wang, J.R. Ran, Y.J. Hao, X.J. Wang, D.S. Zhao, S.Z. Qiao, Nanoscale 7 (2015) 1116–1126.
[38] A. Nag, K. Raidongia, K.P.S.S. Hembram, R. Datt, U.V. Waghmare, C.N.R. Rao, ACS Nano 4 (2010) 1539–1544.
[39] J. Di, J.X. Xia, M.X. Ji, H.P. Li, H. Xu, H.M. Li, R. Chen, Nanoscale 7 (2015) 11433–11443.
[40] J. Di, J.X. Xia, M.X. Ji, B. Wang, S. Yin, Q. Zhang, Z.G. Chen, H.M. Li, ACS Appl. Mater. Interfaces 7 (2015) 20111–20123.
[41] C.Y. Zhi, Y. Bando, C.C. Tang, D. Golberg, J. Am. Chem. Soc. 127 (2005) 17144–17145.
[42] G. Lian, X. Zhang, M. Tan, S.J. Zhang, D.L. Cui, Q.L. Wang, J. Mater. Chem. 21 (2011) 9201–9207.
[43] J. Di, J.X. Xia, Y.P. Ge, H.P. Li, H.Y. Ji, H. Xu, Q. Zhang, H.M. Li, M.N. Li, Appl. Catal. B 168–169 (2015) 51–61.
[44] J. Di, J.X. Xia, S. Yin, H. Xu, L. Xu, Y.G. Xu, M.Q. He, H.M. Li, J. Mater. Chem. A 2 (2014) 5340–5351.
[45] J. Di, J.X. Xia, S. Yin, H. Xu, L. Xu, Y.G. Xu, M.Q. He, H.M. Li, RSC Adv. 4 (2014) 14281–14290.
[46] J. Xiong, W.S. Zhu, H.P. Li, W.J. Ding, Y.H. Chao, P.W. Wu, S.H. Xun, M. Zhang, H.M. Li, Green Chem. 17 (2015) 1647–1656.
[47] X.F. Song, J.L. Hu, H.B. Zeng, J. Mater. Chem. C 1 (2013) 2952–2969.
[48] J. Xiong, W.S. Zhu, H.P. Li, L. Yang, Y.H. Chao, P.W. Wu, S.H. Xun, W. Jiang, M. Zhang, H.M. Li, J. Mater. Chem. A 3 (2015) 12738–12747.
[49] Y.D. Hou, A.B. Laursen, J.S. Zhang, G.G. Zhang, Y.S. Zhu, X.C. Wang, S. Dahl, I. Chorkendorff, Angew. Chem. Int. Ed. 52 (2013) 3621–3625.
[50] M. Zhang, X.J. Bai, D. Liu, J. Wang, Y.F. Zhu, Appl. Catal. B 164 (2015) 77–81.
[51] Y.Y. Zhu, Y.F. Liu, Y.H. Lv, Q. Ling, D. Liu, Y.F. Zhu, J. Mater. Chem. A 2 (2014) 13041–13048.
[52] K. Li, H.B. Zhang, Y.P. Tang, D.W. Ying, Y.L. Xu, Y.L. Wang, J.P. Jia, Appl. Catal. B 164 (2015) 82–91.